

Application of Quenching and Partitioning (Q&P) Processing to Press Hardening Steel

EUN JUNG SEO, LAWRENCE CHO, and BRUNO CHARLES DE COOMAN

Press hardening steel (PHS) has been increasingly used for the manufacture of structural automotive parts in recent years. One of the most critical characteristics of PHS is a low residual ductility related to a martensitic microstructure. The present work proposes the application of quenching and partitioning (Q&P) processing to improve the ductility of PHS. Q&P processing was applied to a Si- and Cr-added Q&P-compatible PHS, leading to a press hardened microstructure consisting of a tempered martensite matrix containing carbide-free bainite and retained austenite. The simultaneous addition of Si and Cr was used to increase the retained austenite fraction in the Q&P-compatible PHS. The Q&P processing of the PHS resulted in a high volume fraction of C-enriched retained austenite, and excellent mechanical properties. After a quench at 543 K (270 °C) and a partition treatment at 673 K (400 °C), the PHS microstructure contained a high volume fraction of retained austenite and a total elongation (TE) of 17 pct was achieved. The yield strength (YS) and the tensile strength were 1098 and 1320 MPa, respectively. The considerable improvement of the ductility of the Q&P-compatible PHS should lead to an improved in-service ductility beneficial to the passive safety of vehicle passengers.

DOI: 10.1007/s11661-014-2316-z

© The Minerals, Metals & Materials Society and ASM International 2014

I. INTRODUCTION

THE use of press hardening steel (PHS) in structural safety-related parts has experienced a rapid growth in the automotive industry, due to increased passenger safety standards which require an improved vehicle intrusion resistance.^[1,2]

Press hardening, also known as hot press forming, hot stamping or die quenching, is a technology to produce automotive ultra-high strength steel (UHSS) parts without spring-back. The hot stamping process can be carried out using two different methods: the direct and the indirect hot stamping method. In the direct hot stamping process, a blank is heated up in a furnace, transferred to the press, and subsequently simultaneously press-formed and quenched in water cooled dies. In the indirect method, the steel sheet is deformed to 90 to 95 pct of its final shape in a forming press with conventional dies prior to austenitization and final die quenching. The indirect method makes it easier to produce parts with larger dimensions and more complicated shapes. The indirect method, which may include several pre-forming presses, is

therefore becoming more widespread.^[1] In recent years, PHS has increasingly been used in automotive car bodies due to its specific advantages, such as an absence of spring-back-related shape effects and the achievement of an ultra-high strength of approximately 1500 MPa. PHS parts are mainly passenger safety-related anti-intrusion parts and structural reinforcements, such as door beams, impact beams, bumpers, pillars, roof rails, and tunnels.^[3] The requirement of an ultra-high strength has, however, lead to concerns about the in-service properties such as fatigue, residual bendability, and toughness.

Quenching and Partitioning (Q&P) processing is a method of stabilizing austenite in steel by quenching the steel to produce a specific volume fraction of martensite and subsequently partitioning the C from martensite to austenite during the partitioning stage. Q&P processing of advanced high strength steel (AHSS) has been shown to improve the ductility of AHSS.^[4] By applying the Q&P processing concept to PHS, the ductility of PHS parts is expected to improve significantly without degradation of the strength. The Q&P-processed PHS might also be applied to parts where additional in-service bending performance is required to avoid catastrophic brittle fracture in passenger car collisions.

The carbide-free bainite microstructure is recognized as a possible constituent for Q&P-processed steel, because the formation of carbide-free bainite leads to the stabilization of a significant retained austenite volume fraction.^[4-7] In previous Q&P studies, the suppression of the bainite formation was thought to be essential,^[7,8] because the bainite formation was considered to be a competing process limiting the partitioning of C from martensite into austenite and thereby reducing the final retained austenite volume fraction.^[7] Carbide-free bainite^[5,9-11] in which the

EUN JUNG SEO and LAWRENCE CHO, Graduate Students, are with the Graduate Institute of Ferrous Metallurgy, Pohang University of Science and Technology, Pohang 790-784, South Korea. BRUNO CHARLES DE COOMAN, Professor, is with the Graduate Institute of Ferrous Metallurgy, Pohang University of Science and Technology, and also Director, with the Materials Design Laboratory, Pohang University of Science and Technology. Contact e-mail: decooman@postech.ac.kr

Manuscript submitted November 26, 2013.

Article published online April 30, 2014

addition of Si leads to the suppression of carbide formation is known to contain C-enriched austenite films, located between bainitic ferrite units. This retained austenite has been shown to result in plasticity enhancement due to the transformation-induced plasticity (TRIP) effect.^[11,12]

In the present work, the Q&P concept was extended to PHS to obtain an UHSS with an enhanced ductility. Figure 1 shows a schematic of a possible process outline and the corresponding heat treatment for the Q&P processing of PHS. The processing is based on the direct hot stamping method. The steel is heated above the A_{c3} temperature in a furnace, transferred to the die-quenching press and subsequently formed. The cooling in the quenching dies is interrupted at a quench temperature, T_Q , in the $M_s - M_f$ temperature range. The austenitized steel transforms in a controlled manner to a microstructure with a specific volume fraction of primary lath martensite α'_p . The partitioning treatment at a temper-

ature $T_P > T_Q$ follows the die-quenching stage in another furnace. In this stage, the carbide-free bainite is formed and simultaneously C diffuses from both the α'_p and the bainitic ferrite into the untransformed austenite. In properly adjusted Q&P processing conditions, the enrichment of austenite with C lowers its M_s temperature and leads to the stabilization of the untransformed austenite upon cooling of the part to room temperature. Otherwise, the remaining austenite transforms to secondary lath martensite α'_s upon cooling to room temperature.

The most commonly used PHS is the 22MnB5 steel grade. It nominally contains 0.22 wt pct C and 1.25 wt pct Mn. B is added to increase the hardenability. Two types of modified 22MnB5 alloys were designed; a Si-added PHS and a Si + Cr-added PHS. Addition of Si allows C to partition into austenite by suppressing the carbide precipitation during the partitioning stage.^[13] Cr acts as an austenite stabilizer during

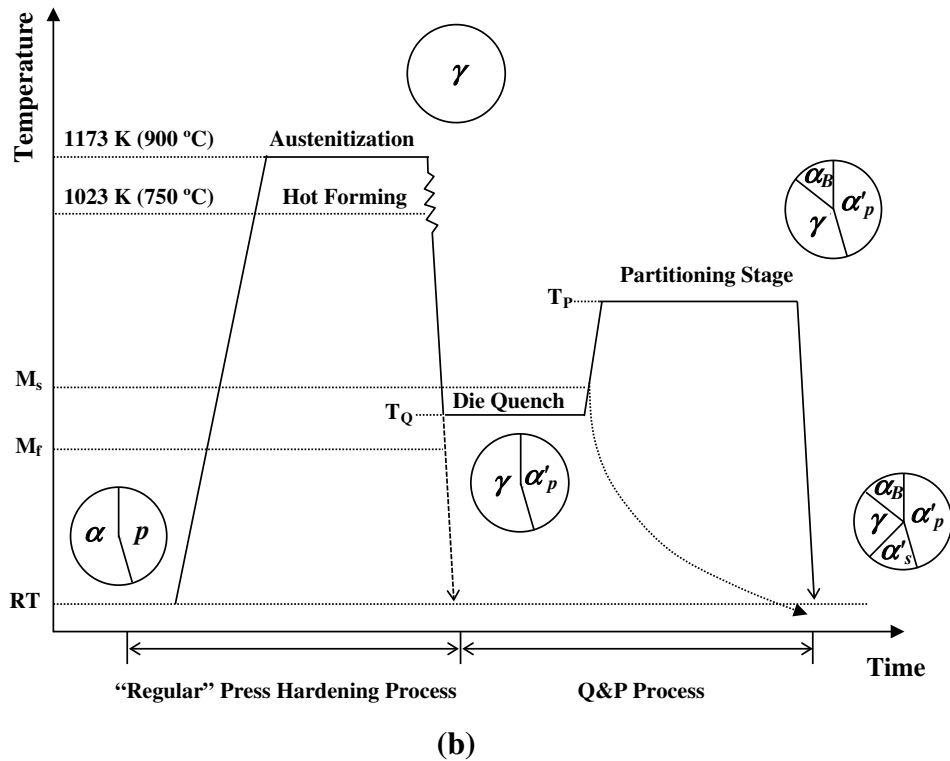
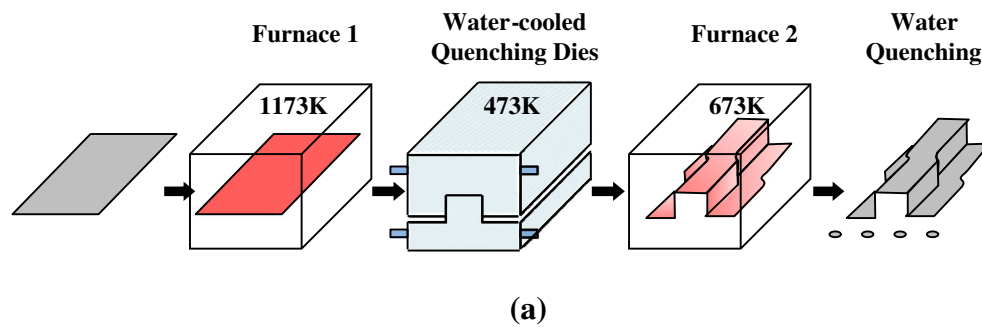


Fig. 1—(a) Schematic of the press hardening process modified for the Q&P processing of the PHS and (b) the corresponding heat treatment cycle. (p : pearlite, γ : austenite, α_B : bainitic ferrite, α'_p : primary martensite, α'_s : secondary martensite).

Q&P processing. Kirchner *et al.*^[14] have shown that although Cr is known to stabilize ferrite at high Cr content, Cr acts as an austenite stabilizer when added in small amounts. Additions of Si and Cr should therefore lead to a room temperature multi-phase microstructure consisting of a martensitic matrix containing carbide-free bainite with C-enriched austenite islands/films. The martensite gives a high strength to the material and the carbide-free bainite with C-enriched austenite contributes to an enhanced elongation and toughness. The present work focuses on the Q&P processing of this new alloy concept for improved in-service properties in automotive applications.

II. EXPERIMENTAL PROCEDURE

The chemical composition of the standard PHS grade, 22MnB5 is listed in Table I. Two modified 22MnB5 alloys were prepared by vacuum induction melting; a Si-added and a Si + Cr-added PHS. The C and Mn contents of both modified PHS were similar to those of the 22MnB5 PHS grade. 1.6 wt pct Si was added to both PHS to suppress the cementite formation. 1.0 wt pct Cr was added to the Si + Cr-added PHS as an essential hardenability agent. Prior to Q&P processing, the industrially cold-rolled Si-added and Si + Cr-added PHS were laboratory heat treated in order to obtain a ferrite-pearlite microstructure prior to the hot press forming simulation. Specimens with dimensions of 10 mm × 5 mm × 1.5 mm were used for dilatometry experiments. The specimens used for Q&P treatments in salt baths were 1.5 mm in thickness, 120 mm in length, and 40 mm in width.

In the present study, the effect of the quench temperature, T_Q , was analyzed for a fixed partitioning temperature (T_P) and time. The T_P temperature was determined by the requirement that C sufficiently partitions into the austenite and, at the same time, that carbide precipitation is avoided. Due to the low diffusivity of C in austenite, the C-enrichment of the austenite is only appreciable for T_P temperatures above 623 K (350 °C) where the long-range diffusion of C in the austenite becomes possible.^[15] Tsuchiyama *et al.*^[16] have demonstrated the presence of M_3C carbides in the martensitic regions of a Q&P-processed AISI martensitic stainless steel partitioned during a treatment at 723 K (450 °C) for 10 minutes. A T_P temperature of 673 K (400 °C) was therefore selected. The partitioning time was selected on the basis of the continuous cooling transformation (CCT) diagram of the PHS shown in Figure 2. The CCT diagram was constructed by dilatometry. The CCT diagrams for the 22MnB5, the Si-

added PHS, and the Si + Cr-added PHS are shown in Figures 2(a) through (c). The partitioning time of 600 seconds was long enough to allow for the formation of a proper amount of carbide-free bainite and leading to a higher volume fraction of C-enriched austenite.

Figure 3 shows a schematic of the thermal cycle used for the Q&P processing of the PHS. Figure 3(a) shows the details of the Q&P cycles carried out on the Si + Cr-added PHS by means of dilatometry experiments, using a Bähr 805 pushrod dilatometer operating in a vacuum of 3×10^{-4} mbar. The specimens were initially fully austenitized for 240 seconds at 1173 K (900 °C). The cooling gas was used during the first quenching stage. The effect of the T_Q temperature on the microstructure evolution was investigated by dilatometry experiments at temperatures in the range from 363 K to 573 K (90 °C to 300 °C) followed by partitioning at 673 K (400 °C) for 180 seconds. Figure 3(b) shows the Q&P heat treatment for the Si-added and the Si + Cr-added PHS carried out in a box furnace and salt baths. These specimens were used for tensile tests and microstructure characterization. The Q&P cycles consisted of annealing at 1173 K (900 °C) for 600 seconds in the box furnace, quenching to a T_Q temperature of 423 K, 473 K, or 543 K (150 °C, 200 °C, or 270 °C) in a first salt bath and partitioning at 673 K (400 °C) for 180 seconds in a second salt bath. The steels were also directly quenched from 1173 K (900 °C) to room temperature, to provide a fully martensitic material for comparison.

The retained austenite content was measured by a METIS magnetic saturation device (Metis Instruments and Equipment NV, Leuven). XRD measurements were carried out by means of a Bruker D8 Advance X-ray diffractometer (Bruker AXS GmbH, Karlsruhe) equipped with a Cu tube. The 2θ range was 40 deg to 100 deg using a step size of 0.02 deg and a measurement time per step of 0.5 seconds. The austenite lattice parameter was determined by the Nelson–Riley method.^[17]

All the specimens used for the microstructural analysis and the XRD measurements were prepared by electro-chemical polishing in a solution of 5 pct $HClO_4$ + 95 pct CH_3COOH in order to minimize possible errors originating from the mechanically induced transformation of retained austenite during sample preparation. Scanning electron microscopy (SEM) and electron backscattering diffraction (EBSD) observation of the microstructure were conducted in a FEI Quanta 3D FEG. The selected specimens were investigated in more detail using a JEOL JEM-2100F FE-Transmission Electron Microscope (JEOL Ltd, Tokyo). Thin foils for TEM were prepared by twin-jet electro-polishing in a solution of 5 pct $HClO_4$ + 95 pct CH_3COOH at room temperature. In order to minimize

Table I. Chemical Composition of the 22MnB5 PHS Grade and the Two Modified PHS Used in the Present Study (Concentrations in Weight Percentage)

	C	Mn	Si	Cr	Ti	N	B
Standard PHS	0.20 to 0.25	1.1 to 1.5	0.1 to 0.4	0.1 to 0.3	0.02 to 0.05	<0.01	0.001 to 0.005
Si-added PHS	0.27	1.50	1.61	0.001	0.027	0.0026	0.0025
Si + Cr-added PHS	0.28	1.46	1.58	0.970	0.023	0.0025	0.0023

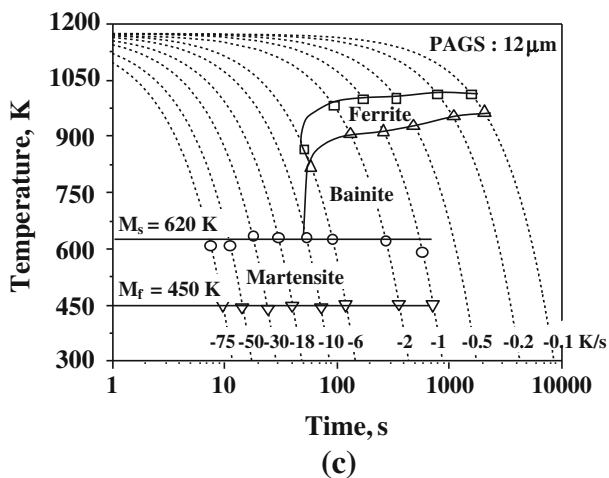
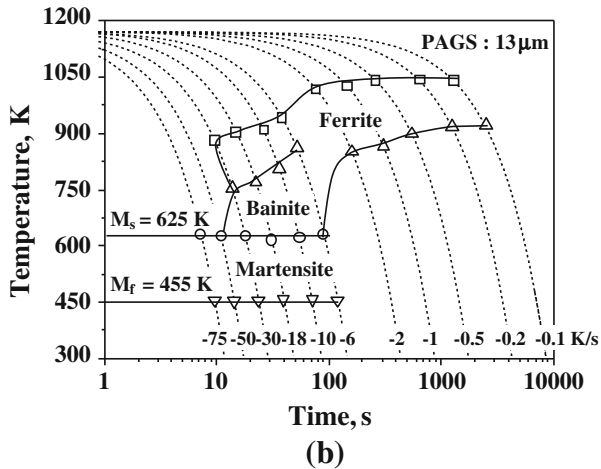
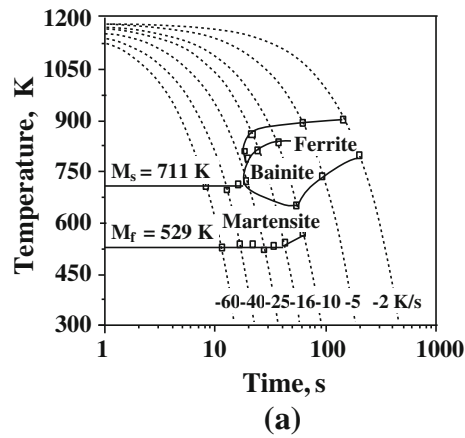


Fig. 2—CCT diagram for (a) 22MnB5 PHS,^[1] (b) Si-added PHS, and (c) Si + Cr-added PHS. PAGES: prior austenite grain size.

the effect of the strong magnetism from the foil specimen on the image quality (IQ), cross-sectional TEM specimens were also prepared by the focused ion beam (FIB) technique in a FEI Quanta 3D FEG. No essential differences were found between the specimens prepared by jet-polishing and by the FIB technique. TEM specimens were observed at an acceleration voltage of 200 kV.

ASTM E8 standard subsize tensile specimens with a gauge length of 25 mm were machined in the rolling direction for each heat treatment. The room temperature mechanical properties were measured in a 2100 Zwick/Roell universal tensile testing machine (Zwick GmbH, Ulm) using a strain rate of 0.005 s^{-1} . Specimens with a length of 5 mm including the fracture surface were taken out from each tested tensile specimen. These specimens were used to measure the retained austenite volume fraction after rupture by means of the magnetic saturation method.

III. RESULTS

A. CCT Diagram of the PHS

The CCT diagrams for the 22MnB5, the Si-added PHS, and the Si + Cr-added PHS are shown in Figures 2(a) through (c). The M_s and M_f temperatures are indicated. The CCT diagrams for the 22MnB5 in Figure 2(a) and the Si-added PHS in Figure 2(b) indicated that the Si addition did not alter the kinetics of the phase transformation appreciably, although it led to a lower M_s temperature and a higher A_{C1} temperature. Cr addition, on the other hand, had a pronounced influence on the kinetics of the austenite decomposition as shown in Figure 2(c). The ferrite transformation range was moved to slightly lower temperatures and became smaller. Cr additions also resulted in wider bainite and martensite transformation ranges, and this resulted in a slightly lower M_s temperature. In addition, Cr remarkably decreased the ferrite transformation start temperature for cooling rates larger than 2 K/s, clearly, albeit indirectly, indicating that Cr acts as an austenite stabilizer at low concentration. An earlier study^[18] found that the addition of Cr enhanced the hardenability of boron-added steel for cooling rates in excess 3 K/s due to the suppression of polygonal ferrite formation at high cooling rates. The CCT diagrams showed that the kinetics of bainitic transformation was delayed for the Si + Cr-added PHS compared to the Si-added PHS.

B. T_Q Dependence of the Retained Austenite Volume Fraction

The influence of the T_Q temperature on the microstructure of the Q&P processed Si + Cr-added PHS was investigated by a series of dilatometry experiments in which specimens were quenched from 1173 K (900 °C) to a T_Q temperature in the range of 363 K to 573 K (90 °C to 300 °C), as shown in Figure 3(a). The quenching was followed by a partitioning stage at 673 K (400 °C) for 180 seconds. Figure 4(a) shows the retained austenite volume fraction, $V_{\gamma \text{ final}}$, as a function of the T_Q temperature. The solid line in Figure 4(a) is the calculated $V_{\gamma \text{ final}}$ using the theoretical model proposed by Speer *et al.*^[19] This model is based on the Koistinen and Marburger equation [1],^[20] which is referred to as the K–M equation. It relates the martensite volume fraction to the undercooling below the M_s temperature ($M_s - T_Q$):

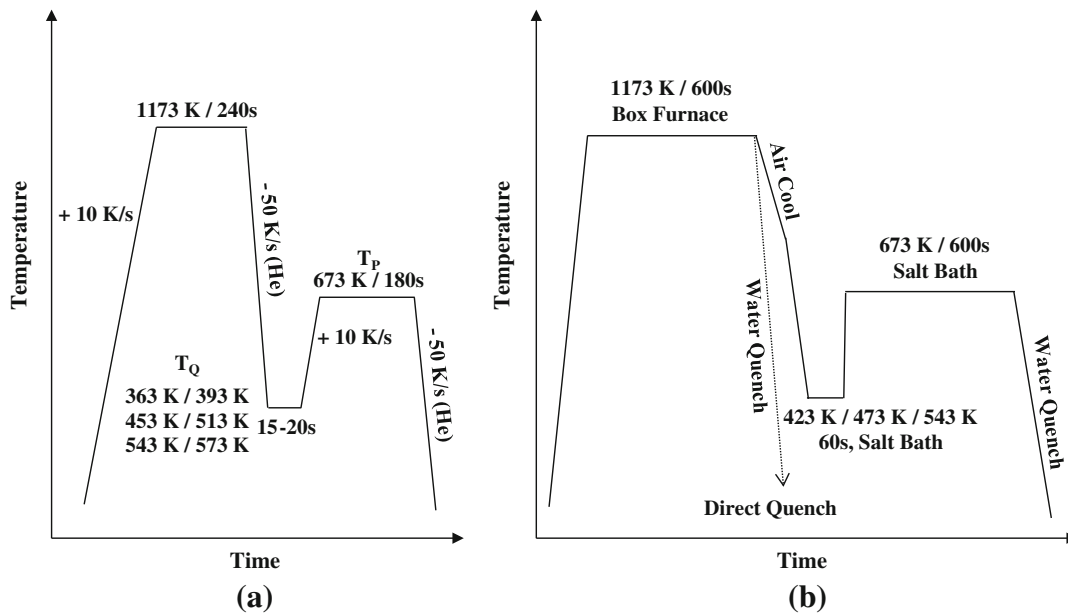


Fig. 3—Schematic of the thermal cycle for the Q&P-processed PHS. (a) Q&P processing for the Si + Cr-added PHS used for the dilatometry experiments. (b) Q&P processing for the Si-added and the Si + Cr-added PHS for the heat treatments in the box furnace and the salt bath.

$$V_{\alpha'} = 1 - \exp[-\alpha(M_s - T_Q)]. \quad [1]$$

Here, $V_{\alpha'}$ is the martensite volume fraction and the constant α is equal to 0.011. The M_s temperatures of the Si-added PHS and the Si + Cr-added PHS were calculated to be 628 K and 615 K (355 °C and 342 °C), respectively, by using the following empirical relationship for the M_s temperature,^[21]

$$M_s = 539 - 423 \cdot C - 30.4 \cdot \text{Mn} - 12.1 \cdot \text{Cr} - 17.7 \cdot \text{Ni} - 7.50 \cdot \text{Mo} + 10 \cdot \text{Co} - 7.5 \cdot \text{Si}. \quad [2]$$

The concentration of each alloy addition is in weight percentage. The M_s temperature of the Si-added and the Si + Cr-added PHS, obtained by dilatometry was 625 K and 620 K (352 °C and 347 °C), respectively. The values of the M_s temperature obtained by means of Eq. [2] and by dilatometry were similar, and the calculated values obtained by means of Eq. [2] were used in the present calculations.

The calculated $V_{\gamma \text{ final}}$ decreased when $T_Q > T_{Q, \text{max}}$ due to the formation of the secondary martensite, α'_s . The volume fraction of α'_s ($V_{\alpha'_s}$) can be determined by means of the K–M equation:

$$V_{\alpha'_s} = (1 - V_{\alpha'}) \cdot [1 - \exp\{-\alpha\{(M'_s - T_Q)\}\}]. \quad [3]$$

The α value is 0.011. The M_s temperature of C-enriched austenite (M'_s) can be expressed by considering the full C partitioning into austenite, *i.e.*, the C content of austenite is equal to the nominal austenite content (C_i) divided by the volume fraction of austenite after the initial quench ($1 - V_{\alpha'}$).

However, the experimental data for $V_{\gamma \text{ final}}$ in Figure 4(a) do not fit the calculated $V_{\gamma \text{ final}}$ obtained by means of Eqs. [1] and [2]. Instead, the measured

$V_{\gamma \text{ final}}$ increased continuously with increasing T_Q . There was no formation of α'_s during the final quenching. This indicates that a higher retained austenite stability was achieved than the one predicted by Eq. [1].

The absence of α'_s formation upon cooling to room temperature was investigated by analyzing the effect of the grain size on the austenite stability. It is known that a small austenite grain size decreases the M_s temperature substantially. García-Junceda *et al.*^[22] reported that the M_s temperature decreased strongly when the austenite grain size was less than 5 μm in an Fe-0.15C-1.9Mn-0.2Si-0.2Cr-0.03Al steel. The model presented above was, therefore, modified to consider both the composition and the grain size of retained austenite. Jimenez-Melero *et al.*^[23] suggested the following equation to calculate the M_s temperature:

$$M_s = M_{s0} - A \cdot C - B \cdot V_{\gamma}^{-1/3}. \quad [4]$$

Here, C is the C content in weight percentage in the retained austenite and V_{γ} is an effective grain volume of the retained austenite. M_{s0} , A, and B are experimentally determined parameters. Equation [4] was modified as follows:

$$M_s = 469 - 423 \cdot C - 60.5 \cdot V_{\gamma}^{-1/3}. \quad [5]$$

Here, the value of M_{s0} and the coefficient related to the C content are taken from Eq. [2]. The numerical coefficient for V_{γ} , suggested by Lee *et al.*^[24] was used. The V_{γ} value was obtained by assuming spherical austenite grains with a diameter of 200 nm.

The dashed line in Figure 4(a) represents $V_{\gamma \text{ final}}$ for the Si + Cr-added PHS calculated using Eqs. [1] and [5]. When the austenite grain size is considered, $V_{\gamma \text{ final}}$ increases with increasing T_Q and there is no formation of α'_s , as the M_s temperature of the austenite is

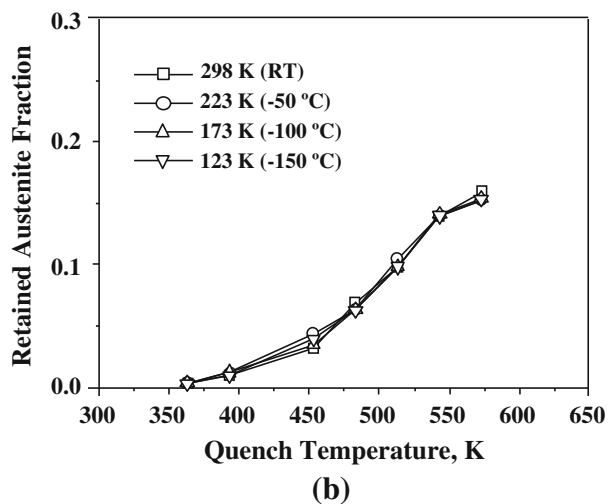
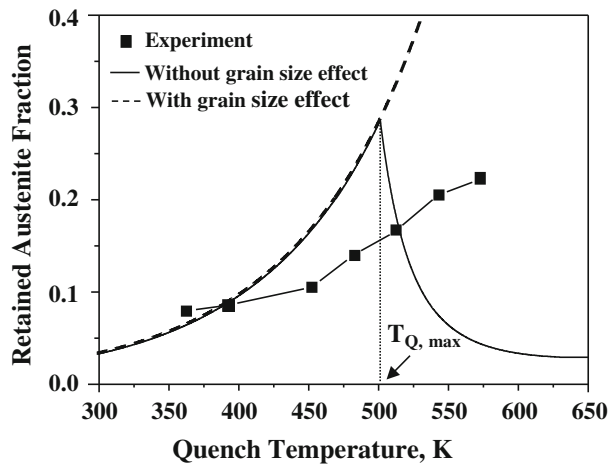


Fig. 4—(a) Calculated and experimentally measured retained austenite volume fractions in the Si + Cr-added PHS as a function of the T_Q temperature for partitioning at 673 K (400 °C). The retained austenite volume fraction was measured by the magnetic saturation method. The solid line is the $V_{\gamma \text{ final}}$ value calculated by means of Eqs. [1] and [2]. The dashed line represents the $V_{\gamma \text{ final}}$ value calculated by means of Eqs. [1] and [5], which considers the effect of the austenite grain size on the M_s temperature. (b) The retained austenite volume fraction measured by magnetic saturation, as a function of the T_Q temperature after subzero cooling in the range from 223 K to 123 K (−50 °C to −150 °C).

significantly lowered by its small grain size. The experimentally measured $V_{\gamma \text{ final}}$ for the Q&P processed Si + Cr-added PHS increased continuously with increasing T_Q .

Figure 4(b) shows $V_{\gamma \text{ final}}$ as a function of the T_Q temperature after subzero treatment in the range of 223 K to 123 K (−50 °C to −150 °C) for the Q&P processed Si + Cr-added PHS. Since the M_s temperature of the retained austenite was substantially lowered by its small grain size, the austenite did not transform to martensite below the room temperature.

The calculated $V_{\gamma \text{ final}}$ and the experimentally measured $V_{\gamma \text{ final}}$ were in better agreement when using Eqs. [1] and [5]. The experimentally measured $V_{\gamma \text{ final}}$ value was lower than the calculated value as indicated in

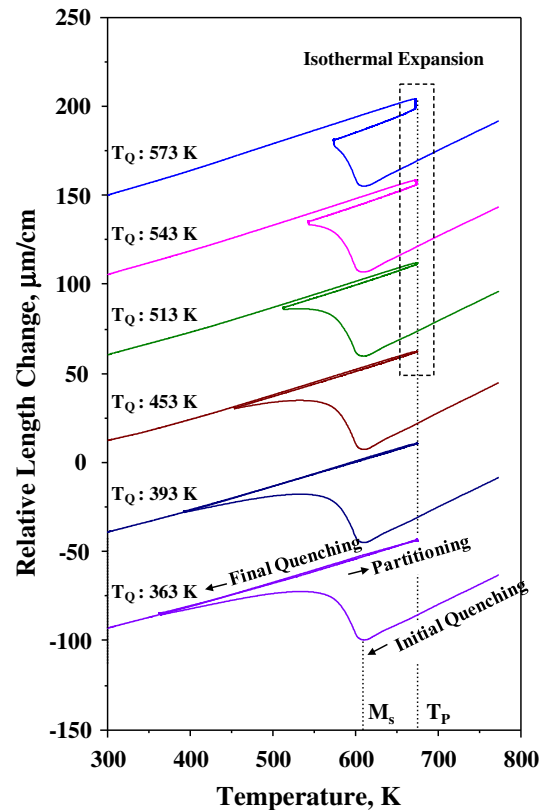


Fig. 5—Relative length change of dilatometry specimens of the Si + Cr-added PHS quenched from 1173 K (900 °C) to different T_Q temperatures in the range from 363 K to 573 K (90 °C to 300 °C), and partition treated at a T_P temperature of 673 K (400 °C) for 180 s. The isothermal expansion resulting from the bainitic transformation during the partitioning stage is indicated by the rectangle.

Figure 4(a). This could be due to the bainitic transformation which takes place in addition to the C partitioning at T_P . Figure 5 shows the dilatometry traces for the Q&P processed Si + Cr-added PHS. There was no volume expansion during the final quenching, which means the α'_s did not form. An isothermal expansion related to the bainitic transformation was, however, observed during the partitioning stage as indicated in Figure 5. The occurrence of the bainite transformation may explain the difference between the calculated and experimentally measured retained austenite volume fraction in Figure 4(a).

C. Microstructure of the Q&P-Processed PHS

On the basis of the dilatometry simulation of the Q&P process, it is clear that austenite partially transforms to martensite during the initial quenching stage at T_Q . At T_P , both the C partitioning from α'_p to austenite and the bainitic transformation of the austenite occurred. In addition, evidence of tempering of the α'_p was observed. Consequently, a final microstructure consisting of a tempered martensite matrix, containing carbide-free bainite and retained austenite was obtained.

Figure 6 shows the microstructures obtained after the Q&P heat treatments presented in Figure 3(b). The specimens were quenched to 543 K (270 °C) and

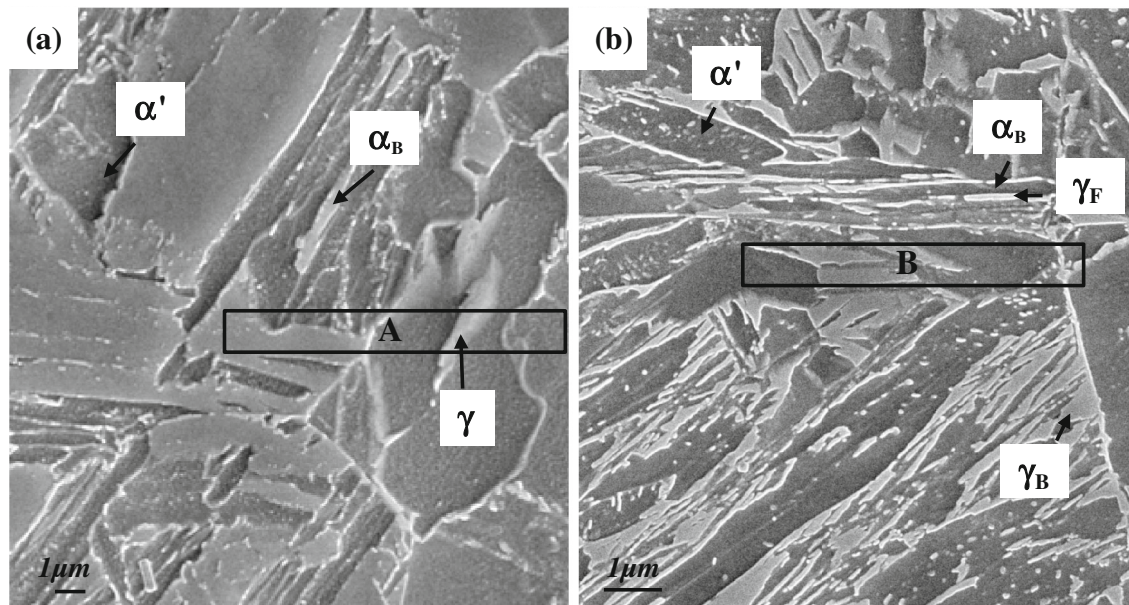


Fig. 6—SEM micrographs of Q&P processed (a) Si-added PHS and (b) Si + Cr-added PHS after quenching to 543 K (270 °C) and partitioning treated at 673 K (400 °C) for 600 s. γ_F , γ_B , α_B , and α' represent film-shape retained austenite, blocky-shape retained austenite, carbide-free bainite, and tempered martensite, respectively. The areas labeled A and B were used for TEM specimens prepared by the FIB technique.

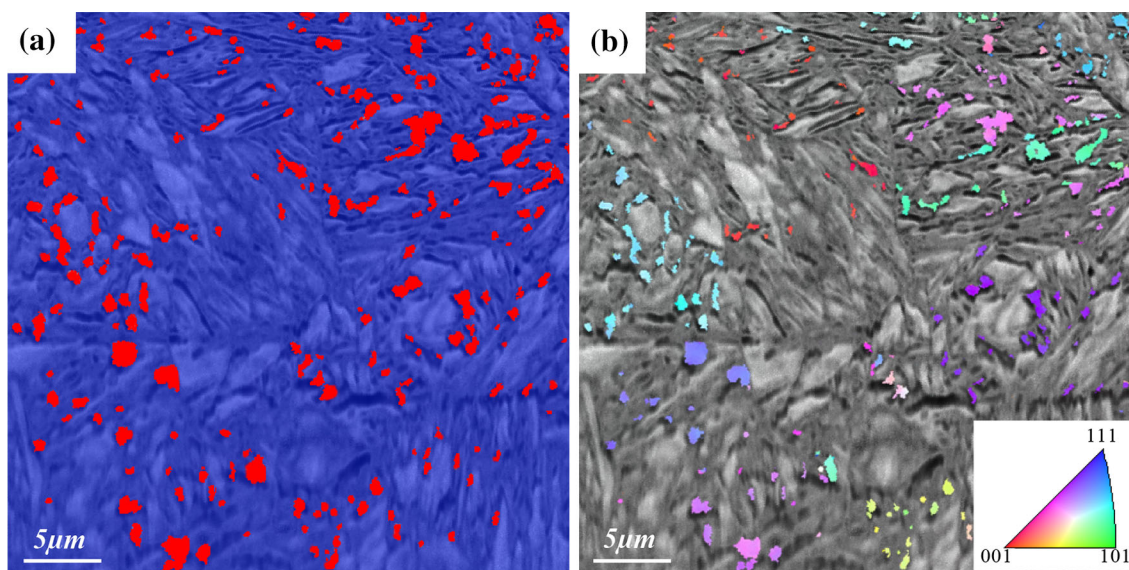


Fig. 7—EBSD analysis of the microstructure of the Q&P processed Si + Cr-added PHS obtained by austenitizing, quenching to 543 K (270 °C) and partitioning treated at 673 K (400 °C) for 600 s. (a) Combined IQ map and color-coded phase map in which blue corresponds to body-centered cubic (bcc) crystal structures (martensite and bainite) and red corresponds to a face-centered cubic (fcc) crystal structure (austenite). (b) Combined IQ map and austenite phase map. The inset shows the inverse pole-figure map for the austenite phase.

partition treated at 673 K (400 °C) for 600 seconds. Both Q&P processed Si-added and Si + Cr-added PHS had a microstructure with a tempered martensite matrix, carbide-free bainite, and austenite islands. The retained austenite volume fraction was 0.11 for the Q&P processed Si-added PHS. A much larger retained austenite volume fraction of 0.20 was measured for the Q&P processed Si + Cr-added PHS. The retained austenite was present both as a film between bainitic laths and as a larger blocky phase (Figure 6(b)). The particles with a

bright contrast in the SEM micrograph of Figure 6(b) of the Q&P processed Si + Cr-added PHS are mainly carbides. The retained austenite was identified by both selected area diffraction in TEM and EBSD analysis. Figure 7 shows EBSD results of the Q&P processed Si + Cr-added PHS. Figure 7(a) shows a combined IQ map and color-coded phase map. Figure 7(b) shows a combined IQ map and inverse pole-figure map of the austenite grains. Austenite grains with the same crystallographic orientation which originated from the same

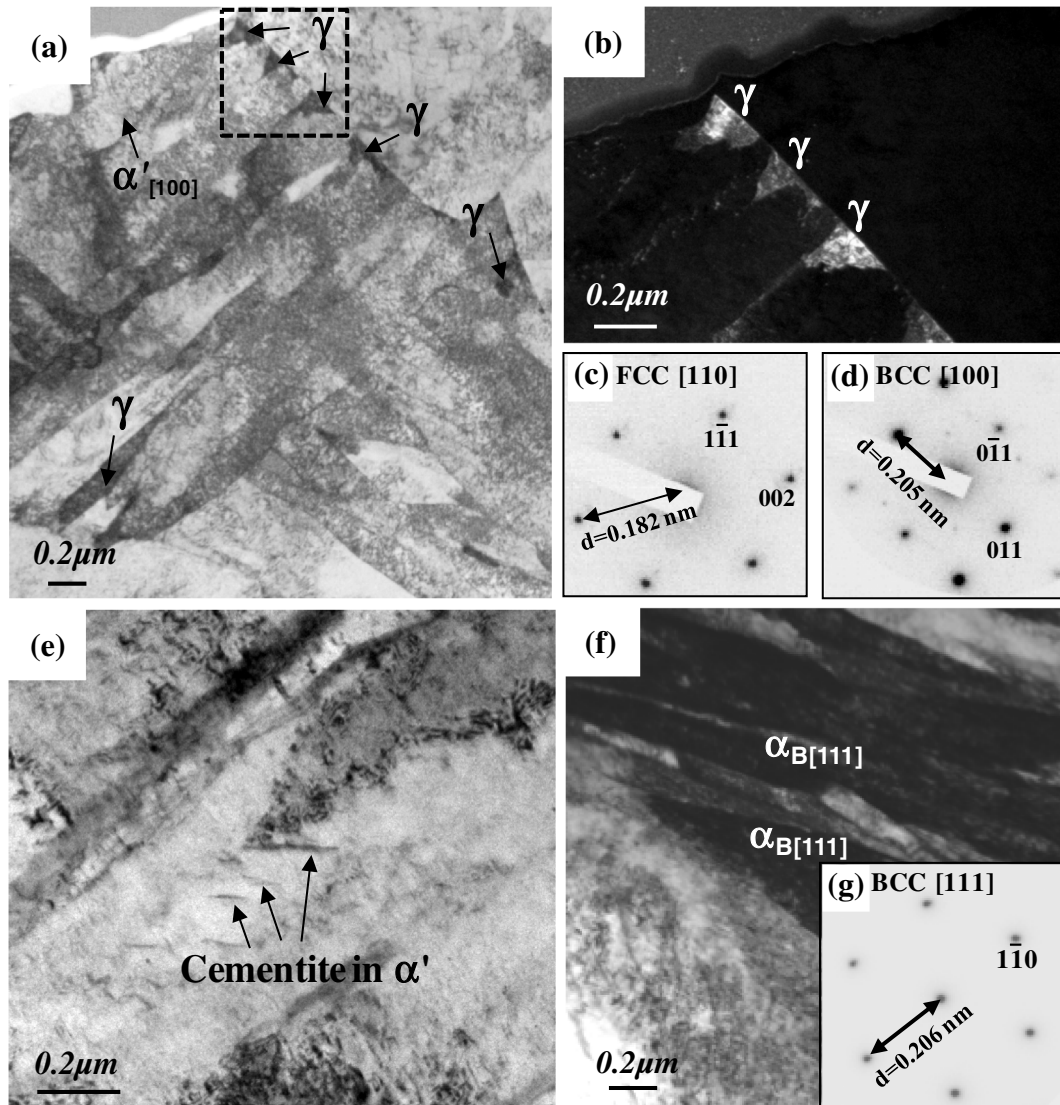


Fig. 8—TEM micrographs of the Q&P processed Si-added PHS obtained by a quench to a T_Q temperature of 543 K (270 °C) and partitioning treated at 673 K (400 °C) for 600 s. (a) through (d) results obtained with a TEM specimen prepared by the FIB technique. It includes the retained austenite area labeled A in Fig. 6(a). (e) through (g) results obtained on a thin foil specimen prepared by jet-polishing. γ , α_B , and α' represent retained austenite, carbide-free bainite, and tempered martensite, respectively. (a) Bright field (BF) image of the bainite containing retained austenite. (b) Dark field (DF) image of the retained austenite in (a) using the $(002)_\gamma$ reflection. (c) Diffraction pattern of the retained austenite in (a). (d) Diffraction pattern of the tempered martensite in (a). (e) BF TEM micrograph showing cementite particles embedded in the tempered martensite. (f) BF image of the carbide-free bainite. (g) Diffraction pattern of the carbide-free bainite in (f).

prior austenite grain can be observed in Figure 7(b). The dark region in Figure 7(b) corresponds to the grain boundaries with a low IQ. The EBSD technique was not able to detect the film-type retained austenite distributed along the lath boundaries due to the instrumental resolution limitation.

Figure 8 shows TEM micrographs of the Q&P processed Si-added PHS. Figure 8(a) shows a cross-sectional view of TEM specimens prepared by the FIB technique. The retained austenite in the area labeled “A” in Figure 6(a) was selected for the FIB specimen preparation. The microstructure of the Q&P processed Si-added PHS consisted of a tempered martensite matrix, carbide-free bainite, and retained austenite. Figure 8(b) shows a dark field micrograph of the

retained austenite present along the grain boundaries. Figures 8(e) and (f) clearly show the difference between tempered martensite and carbide-free bainite. Figure 8(e) shows carbides embedded in the tempered martensite lath. Figure 8(f) shows carbide-free bainite with a lath width of about 200 nm. Weak diffraction spots in the diffraction pattern of tempered martensite in Figure 8(d) indicate the presence of carbides. In contrast, no carbide reflections were present in the diffraction patterns obtained from the bainitic ferrite in the carbide-free bainite in Figure 8(g).

Figure 9 shows TEM micrographs of the Q&P processed Si + Cr-added PHS. Figure 9(a) shows a cross-sectional view of a TEM specimen prepared by the FIB technique. The specimen includes the area

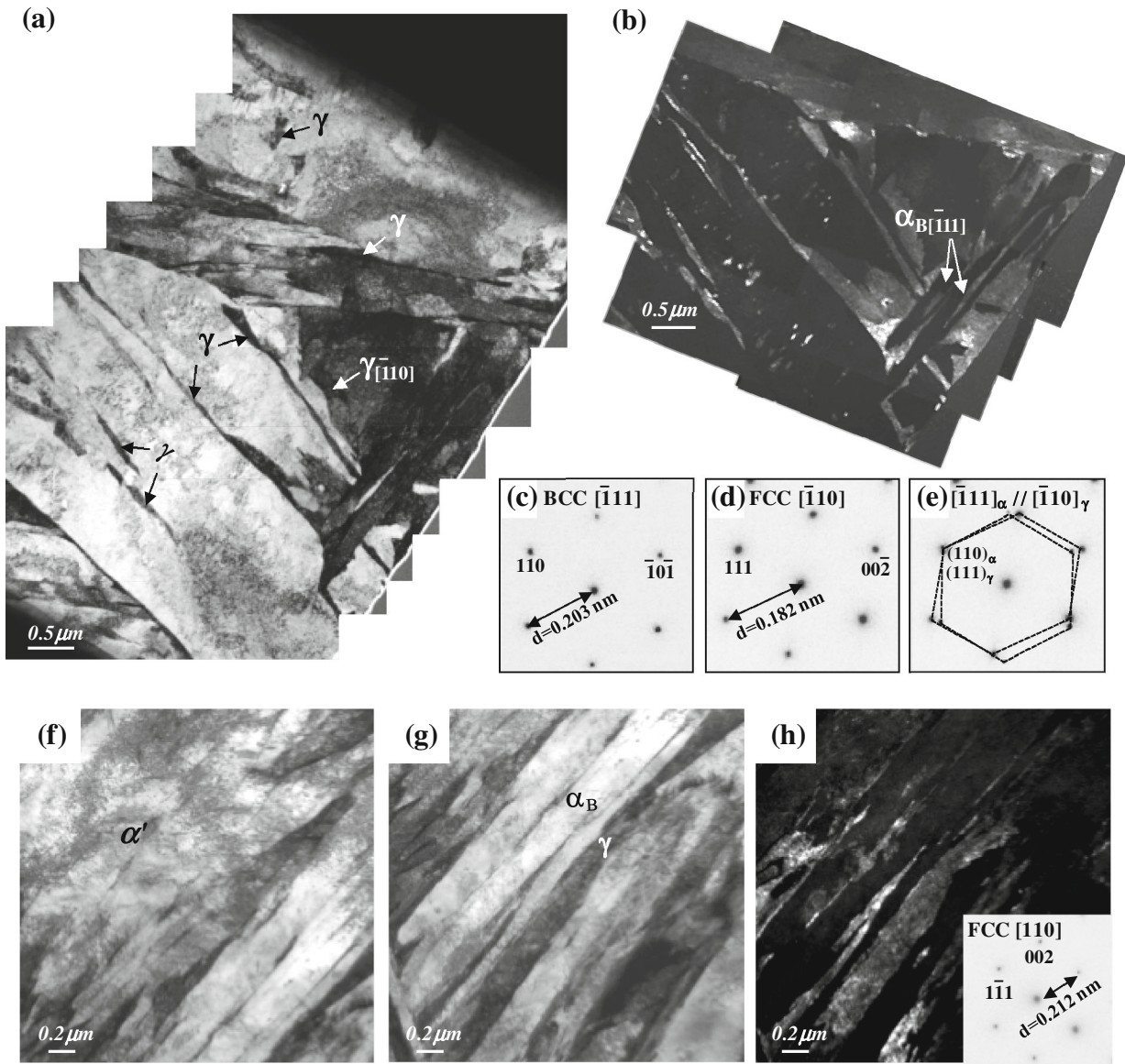


Fig. 9—TEM micrographs of the Q&P processed Si + Cr-added PHS obtained by a quench to a T_Q temperature of 543 K (270 °C) and partitioning treated at 673 K (400 °C) for 600 s. (a) through (e) results obtained with a TEM specimen prepared by the FIB technique. The retained austenite area is labeled B in Fig. 6(b). (f) through (h) results obtained on a thin foil specimen prepared by jet-polishing. γ , α_B , and α' represent retained austenite, carbide-free bainite, and tempered martensite, respectively. (a) BF image. (b) DF image of the retained austenite in (a) using the $(00\bar{2})_\gamma$ reflection. (c) Diffraction pattern of the bainitic ferrite in the carbide-free bainite. (d) Diffraction pattern of the retained austenite in (a). (e) SADP indicating the Kurdjumov–Sachs orientation relationships, $[\bar{1}11]_\alpha // [\bar{1}10]_\gamma$ and $(110)_\alpha // (111)_\gamma$ between retained austenite and bainitic ferrite in the carbide-free bainite. (f) Dislocated tempered martensite. (g) Bainitic ferrite and retained austenite in the carbide-free bainite. (h) DF image of the retained austenite in (g) using the $(002)_\gamma$ reflection.

labeled “B” in Figure 6(b) which contained retained austenite. The microstructure of the Q&P processed Si + Cr-added PHS consisted of a tempered martensite matrix, carbide-free bainite, and retained austenite. Figure 9(b) shows a dark field image of the retained austenite present along the grain boundaries. Compared to the Q&P processed Si-added PHS, a much larger retained austenite volume fraction was present in the Q&P processed Si + Cr-added PHS. Film-type retained austenite was also present along the grain boundaries. This confirms that the thin boundary phase with a bright contrast in the SEM image of Figure 6(b) was austenite.

It should be pointed out that small blocky austenite grains were also present. These austenite grains sometimes appeared to be carbides during SEM observation due to their shape. Suzuki *et al.*^[25] reported that the shapes of cementite and retained austenite formed during isothermal bainitic transformation were very similar and that it was difficult to distinguish them from each other. Figures 9(c) and (d) show the diffraction pattern of the bainitic ferrite in the carbide-free bainite and the retained austenite, respectively. The diffraction pattern shown in Figure 9(e) reveals that a Kurdjumov–Sachs orientation relationship existed between the

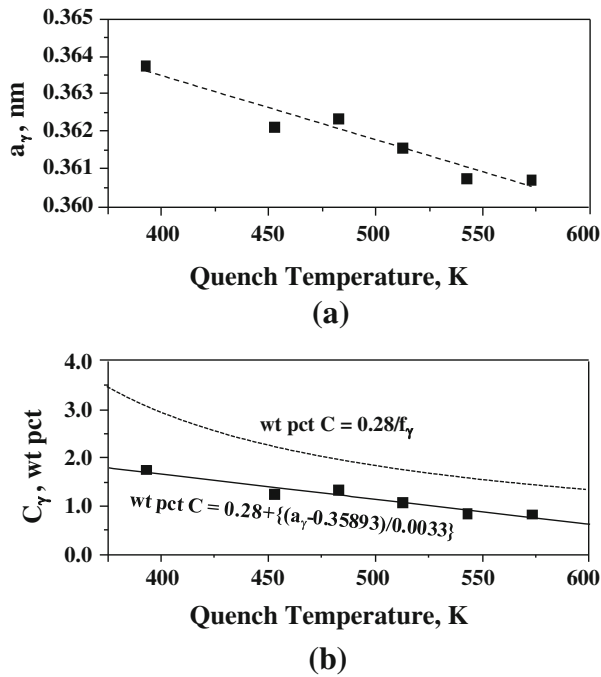


Fig. 10—(a) Room temperature lattice parameter of the retained austenite, a_γ , in the Q&P processed Si + Cr-added PHS partition treated at 673 K (400 °C) for 180 s as a function of the T_Q temperature. (b) Quench temperature dependence of the C content of austenite, C_γ , based on the XRD austenite lattice parameter measurements. The solid line is based on Eq. [6]. The C content derived for the full partitioning assumption is shown (dashed line) for comparison.

bainitic ferrite laths in the carbide-free bainite and the retained austenite. Figure 9(f) shows the presence of a high dislocation density in the microstructure of the tempered martensite matrix. Figure 9(g) shows the close association between the bainitic ferrite and the retained austenite in the carbide-free bainite. The dark field image in Figure 9(h) clearly reveals the presence of the retained austenite.

D. Retained Austenite C Concentration

The results of Section III-C indicated that the features of the high strength microstructures obtained after Q&P processing. A higher volume fraction of retained austenite was present in the Q&P processed Si + Cr-added PHS as compared to the Q&P processed Si-added PHS. In order to examine the C concentration of austenite in the Q&P processed Si + Cr-added PHS, the room temperature retained austenite lattice parameter was measured as a function of the T_Q temperature.

C is the main alloying element utilized for austenite stabilization in Q&P processing. The C content of austenite is therefore particularly important. This C content can be determined by means of the room temperature measurement of the lattice parameter of the retained austenite, a_γ , and relationship between the austenite lattice parameter and its C content. Figure 10(a) shows the austenite lattice parameter of the Q&P processed Si + Cr-added PHS partition treated at 673 K (400 °C) for 180 seconds as a function of the

T_Q temperature. The lattice expansion associated with C partitioning to austenite increased as the T_Q temperature decreased. The austenite lattice parameter was converted to the austenite C content in using the following empirical relationship.^[26]

$$a_\gamma(\text{nm}) = 0.35780 + 0.0033 \cdot C + 0.000095 \cdot \text{Mn} \\ - 0.00002 \cdot \text{Ni} + 0.00006 \cdot \text{Cr} + 0.00056 \cdot \text{Al} \\ + 0.00031 \cdot \text{Mo} + 0.00018 \cdot \text{V}. \quad [6]$$

Substitutional atom diffusion is very slow at temperatures involved in the Q&P stage of Q&P processing. C is therefore the only element responsible for the lattice parameter variation, and only the C content dependence of the austenite lattice parameter in Eq. [6] was utilized. The room temperature lattice parameter of the austenite with the composition of the Si + Cr-added PHS was taken as 0.35893 nm. The possible effect of internal stresses on the lattice parameter of austenite was neglected. Figure 10(b) shows the C content of the retained austenite based on the XRD austenite lattice parameter measurements. The straight line represents the C contents in austenite based on Eq. [6]. The dotted line in Figure 10(b) indicates the C content for full partitioning, *i.e.*, when all the C are assumed to partition from α'_p to the untransformed austenite, for comparison. The C did clearly not partition fully into austenite. This was confirmed by the observation of carbides in the microstructural analysis. In addition, some C may remain segregated at martensite lattice defects.

E. Mechanical Properties of Q&P-Processed PHS

Figure 11 shows engineering stress–strain curves for Q&P processed Si-added and Si + Cr-added PHS quenched to a T_Q temperature of 423 K, 473 K, and 543 K (150 °C, 200 °C, and 270 °C) and partition treated at 673 K (400 °C) for 600 seconds. The curves for the PHS directly quenched from 1173 K (900 °C) to room temperature are also shown. The typical values for the ultimate tensile strength (UTS) and the TE of a 22MnB5 PHS are indicated, for comparison. Figure 12 and Table II summarize the tensile properties of Q&P processed Si-added and Si + Cr-added PHS, averaged from three tests, as a function of the T_Q temperature. The light gray bands in Figure 12 indicate the typical range for the YS, UTS, and TE of the 22MnB5 PHS. The Q&P processed Si + Cr-added PHS exhibited a significantly improved plasticity, compared to the PHS directly quenched to room temperature. The TE of the PHS directly quenched to room temperature was about 5 pct. The Q&P processed Si + Cr-added PHS had a TE of 17 pct. The TE values of Q&P-processed PHS were higher than for 22MnB5 PHS at a similar high strength level. For both Q&P processed Si-added and Si + Cr-added PHS, the ductility was significantly improved at increased T_Q temperatures. This was due to larger volume fractions of austenite in the specimens quenched to a higher T_Q temperature. These results support the

fact that the retained austenite volume fraction was significantly influenced by the T_Q temperature.

The Q&P processed Si + Cr-added PHS had superior mechanical properties compared to the Q&P processed Si-added PHS. Although the mechanical properties of the Si-added and Si + Cr-added PHS directly quenched to room temperature were very similar, a beneficial effect of Cr was clearly observed when the PHS was Q&P processed. When the T_Q temperatures were of 423 K and 473 K (150 °C and 200 °C), the YS, the UTS, and the TE of the Q&P processed Si + Cr-added PHS were superior to those of the Q&P processed Si-added PHS. When the T_Q temperature was 543 K (270 °C), the TE of the Q&P processed Si + Cr-added PHS increased to 17 pct, while the UTS values for both steels were similar. However, the YS of the Q&P processed Si + Cr-added PHS was relatively low, because it had the highest volume fraction of retained austenite when quenched to 543 K (270 °C) and partition treated at 673 K (400 °C) for 600 seconds.

The work hardening behavior for the Q&P processed Si-added PHS and Si + Cr-added PHS is compared in Figure 13. Figures 13(a) and (b) show the true stress–strain curves and the work hardening curves for Q&P processed Si-added PHS and Si + Cr-added PHS, respectively. Figures 13(c) and (d) show the retained austenite volume fraction for Q&P processed Si-added PHS and Si + Cr-added PHS, respectively, before and after strain. For both PHS, the work hardening increased when the T_Q temperature increased. The Q&P processed Si + Cr-added PHS showed a much higher work hardening rate compared to the Q&P

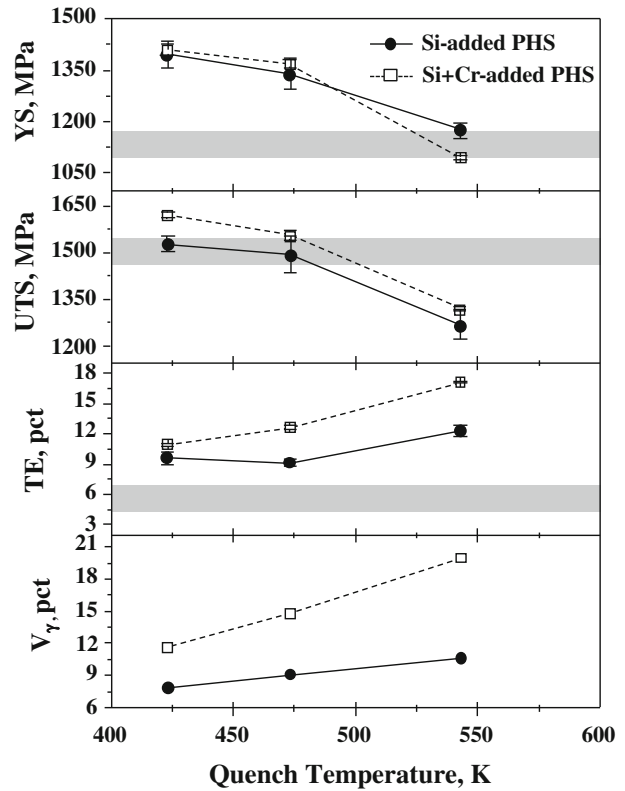


Fig. 12— T_Q temperature dependence of the tensile properties of Q&P processed Si-added and Si + Cr-added PHS partition treated at 673 K (400 °C) for 600 s. The light gray bands indicate typical ranges for the YS, UTS, and TE of the standard 22MnB5 PHS grade.

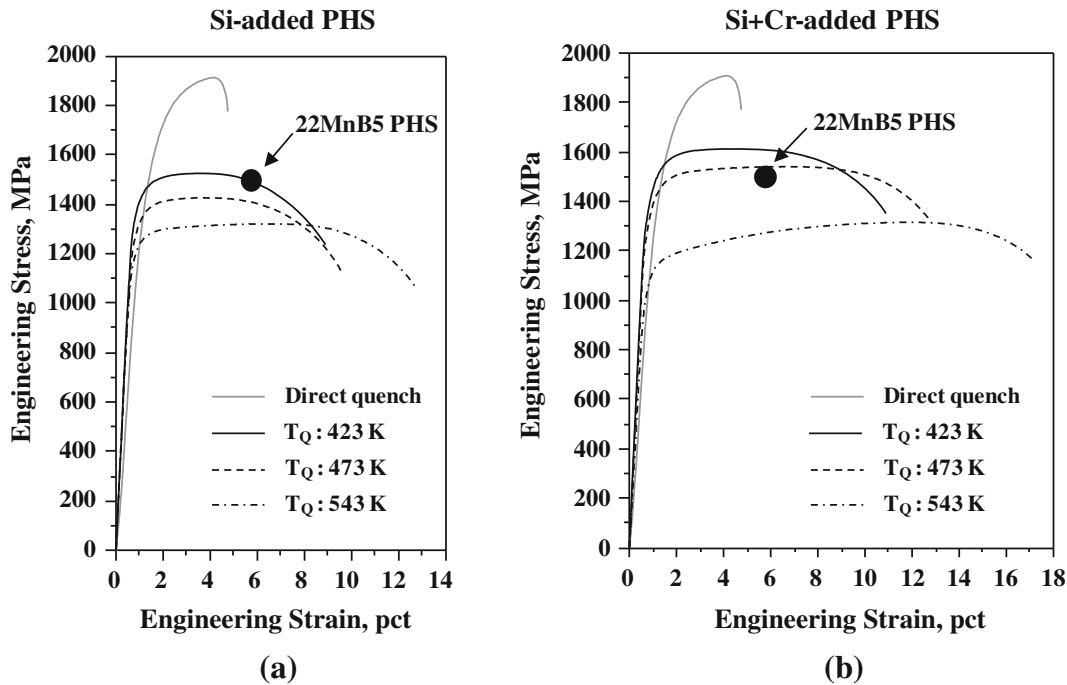


Fig. 11—Room temperature stress–strain curves for Q&P-processed PHS. (a) Si-added PHS. (b) Si + Cr-added PHS. The steels were quenched to 423 K, 473 K, and 543 K (150 °C, 200 °C, and 270 °C) and partition treated at 673 K (400 °C) for 600 s. The curves for the PHS directly quenched from 1173 K (900 °C) to room temperature are also shown, for comparison. Typical value range for the UTS and the TE of a 22MnB5 PHS is indicated.

Table II. T_Q Dependence of the Tensile Properties of the Q&P-Processed PHS. The Steels Were Partition Treated at 673 K (400 °C) for 600 s

T_Q [K (°C)]	YS ($\sigma_{0.2}$) (MPa)	UTS (MPa)	Uniform Elongation (Pct)	TE (Pct)	V_7
Si-added PHS					
423 (150)	1396	1528	3.0	9.6	0.08
473 (200)	1340	1493	3.0	9.1	0.09
543 (270)	1178	1269	5.3	12.3	0.11
Si-Cr-added PHS					
423 (150)	1410	1621	3.7	10.9	0.12
473 (200)	1370	1556	5.8	12.6	0.15
543 (270)	1098	1321	11	17.1	0.20

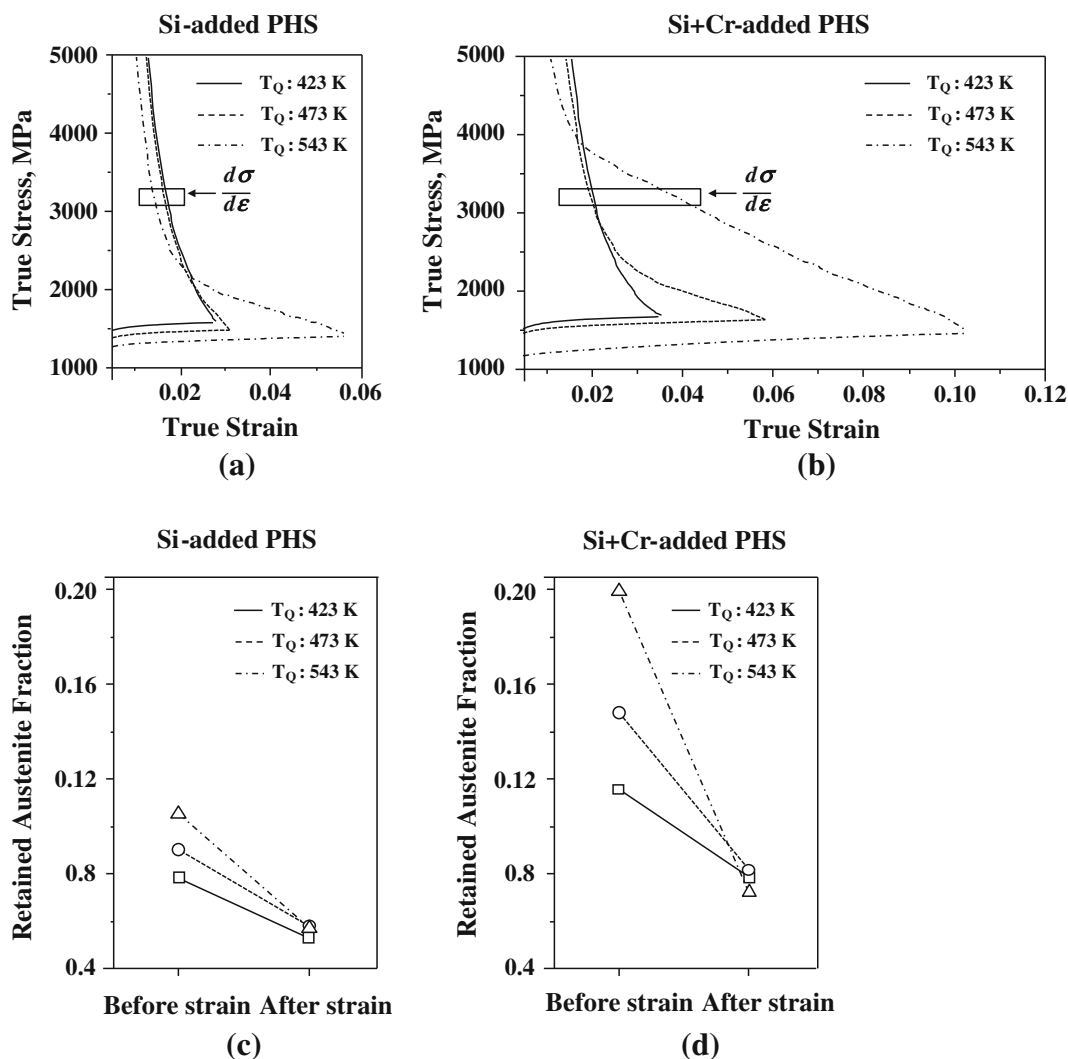


Fig. 13—True stress–strain and work hardening rate curves for (a) Q&P processed Si-added PHS and (b) Si + Cr-added PHS. Retained austenite fraction before and after strain for (c) Q&P processed Si-added PHS and (d) Si + Cr-added PHS.

processed Si-added PHS. When the T_Q temperature was 543 K (270 °C), the work hardening rate and the uniform elongation of the Q&P processed Si + Cr-added PHS significantly increased. This was due to the strain-induced transformation of the austenite to martensite (TRIP effect).

IV. DISCUSSION

In the original Q&P concept, the retained austenite volume fraction is normally seen to decrease for quenching temperatures above the $T_{Q,max}$ temperature due to formation of secondary martensite, α'_s . The absence of bainite formation is usually considered to be

essential, because it reduces the final retained austenite volume fraction by limiting the C partitioning. The results of present study, however, seem to differ somewhat from the original model of Q&P processing.

There were two differences between the original Q&P concept and the results of the present study: (a) bainite was formed during the partitioning stage and (b) α'_s did not form during the final quench. The results in the present study indicated that as the T_Q temperature increased, the retained austenite volume fraction increased continuously without the formation of α'_s upon cooling to room temperature. This is likely due to the effect of the small austenite grain size. The reason for the austenite grains being small may be related to the bainite formation. In Section III-A, the model prediction showed that if the grain size effect was considered, α'_s did not form during the final quenching. This observation suggests that the M_s temperature of the austenite was significantly lowered due to its small grain size, resulting in an increased stability of austenite against the martensite transformation in the final quenching. As a result, the α'_s did not form for $T_Q > T_{Q,max}$ temperature when the Si-added and the Si + Cr-added PHS steels were Q&P processed.

Both Q&P processed Si-added and Si + Cr-added PHS had microstructures with a tempered martensite matrix, carbide-free bainite, and retained austenite. The Q&P processing resulted in considerable amounts of retained austenite in the PHS. The retained austenite volume fractions for Q&P processed Si-added and Si + Cr-added PHS were 0.11 and 0.20, respectively. The retained austenite was present both as a film between bainitic laths and as a larger blocky phase. The tempered martensite and the carbide-free bainite can be distinguished in TEM observations by two methods. The first method is to observe the presence or absence of carbides. Bhadeshia and Edmonds^[12] have shown that carbide-free bainite forms when the Si content is higher than 1.6 wt pct. It is known that Si effectively suppresses cementite formation. This effect is usually explained by the fact that Si has a low solubility in cementite, and that the nucleation and growth of cementite requires Si to be rejected from the transforming volume. This retards the kinetics of carbide growth. In contrast, Si additions do not effectively suppress the formation of transition carbides,^[6,27] a phenomenon which is very likely due to the higher solubility of Si in transition carbides. In the present study, Si suppressed the cementite formation during the partitioning stage. This resulted in the formation of carbide-free bainite. However, transition carbides were still formed in the martensite during the quenching or the reheating from the T_Q to the T_P temperature. The bcc phase containing carbides is, therefore, tempered martensite. The morphology also offers a clue to the identity of the phase. Both bainite and martensite have a lath morphology. The morphology of the carbide-free bainite, however, often contains thin inter-lath retained austenite films due to the specifics of the bainite growth mechanism. The width of the laths of bainitic ferrite in carbide-free bainite has been reported to be about 200 nm in high Si steels.^[13] Tempered martensite also tends to have a higher

dislocation density in its microstructure due to its lower formation temperature.

The enrichment of C to the austenite is considerable when compared to the nominal C content of the PHS. This suggests that C was also partitioned from martensite to austenite during the Q&P processing and that the formation of carbide-free bainite contributed to the C-enrichment of austenite. A maximum C content of approximately 1.8 wt pct was obtained for $T_Q = 393$ K (120 °C). The C content dependence of the M_s temperature was obtained by means of Eq. [2]. In Q&P processed Si + Cr-added PHS, the C content of the retained austenite exceeded 1.1 wt pct and the M_s temperature was below room temperature, indicating austenite stabilization at room temperature. For $T_Q < 513$ K (240 °C), the C content of the retained austenite exceeded 1.1 wt pct. As a consequence, no α'_s was formed during the final quenching. Despite the fact that, for $T_Q > 513$ K (240 °C), the austenite C content was less than 1.1 wt pct, no α'_s was formed during the final quenching. Further cooling to subzero temperatures also indicated that the M_s temperature was much lower than room temperature (Figure 4(b)). This observation suggests that the stability of retained austenite was influenced by other factors. Samek *et al.*^[28] reported that the stability of retained austenite is not only determined by the composition of the retained austenite. The size, the morphology, and the distribution of retained austenite in the microstructure are also important. They suggested that the austenite stability may be increased when the austenite islands are embedded in a hard matrix. In the Q&P processed Si + Cr-added PHS, the austenite was present as very fine grains embedded in either martensite or bainitic ferrite (Figures 7, 9). Therefore, both the grain size and the morphology of the austenite contributed to the stability of retained austenite in the present case.

The mechanical properties of the Q&P processed Si-added and Si + Cr-added PHS were influenced by the retained austenite volume fraction. Retained austenite is a ductile phase compared to bainitic ferrite and martensite, so its presence is expected to enhance ductility. Microstructural observations revealed that the austenite islands were homogeneously distributed in the form of thin films along the grain boundaries in the Q&P processed Si + Cr-added PHS. This fact explains why the TE and the UTS of the Q&P processed Si + Cr-added PHS were higher than those of the Q&P processed Si-added PHS. In particular, the Q&P processed Si + Cr-added PHS quenched to 543 K (270 °C) exhibited the best combination of strength and ductility (YS = 1098 MPa, UTS = 1320 MPa, and TE = 17 pct). This Q&P-processed PHS had a pronounced work hardening behavior as shown in Figure 13(b). This results from an optimal combination of both the volume fraction and the stability of the retained austenite. The Q&P processed Si + Cr-added PHS quenched to a $T_Q > 543$ K (270 °C) exhibited the highest volume fraction of retained austenite, 0.20, whereas the C content of the austenite was relatively low. This is reasonable because, if the retained austenite volume fraction is high, the amount of C which can be

partitioned per unit volume of austenite will be lower, resulting in a less stable retained austenite. The volume fraction of retained austenite transformed to martensite during the straining was largest for the Q&P processed Si + Cr-added PHS quenched to a T_Q of 543 K (270 °C), as shown in Figure 13(d). It is believed that this resulted in a more pronounced TRIP effect. In other words, the combination of a relatively lower austenite stability and a high volume fraction of retained austenite resulted in a higher rate of work hardening and a significantly improved ductility.

The main effect of the Si addition on the microstructure was to retain C in solid solution by suppression of carbide formation during the partitioning stage. This also leads to the formation of carbide-free bainite by C-enrichment in the inter-lath austenite films.

The synergetic effect of Si and Cr addition was significant. The Q&P processed Si + Cr-added PHS had a higher retained austenite volume fraction than the Q&P processed Si-added PHS. This leads to an improvement of the mechanical properties. Jirková *et al.*^[29] reported that the tensile properties of Q&P processed Cr-added steel were superior to that without Cr addition. Suzuki *et al.*^[25] also reported that as Cr and Si concentrations increased, the amount of retained austenite during bainitic transformation increased. They suggested that this was due to increase of C concentration of untransformed austenite by suppression of cementite precipitates during the bainitic transformation. They did, however, not give a reason for the effect of Cr.

The effect of Cr on the retained austenite volume fraction may be due to the following:

- (1) Cr decreases the M_s temperature of austenite.
- (2) Cr delays the bainitic transformation.
- (3) At low concentrations, Cr acts as an austenite stabilizer.

A decrease of the M_s temperature resulting from the Cr addition results in a higher retained austenite volume fraction for the Si + Cr-added PHS than for the Si-added PHS. According to the K–M equation, the martensite volume fraction is determined only by the undercooling below the M_s temperature. That is, a higher M_s temperature results in a higher martensite volume fraction for a given T_Q temperature. The M_s temperature of the Si-added PHS was higher than that of the Si + Cr-added PHS as shown in the CCT diagrams. Therefore, the austenite volume fraction in the Si + Cr-added PHS after the initial quenching to a T_Q temperature was higher than for the Si-added PHS.

Cr additions are known to delay the bainitic transformation. This makes microstructure control easier since the partitioning time can be longer and excessive amounts of bainitic ferrite can be avoided. Although carbide-free bainite was intentionally formed in a controlled manner in this study, limiting the kinetics of the bainite formation is important because bainite is an austenite decomposition reaction. Figure 14 shows dilatometric results for both the Si-added PHS and the Si + Cr-added PHS during an isothermal holding at 673 K (400 °C) for 2000 seconds after austenitization at

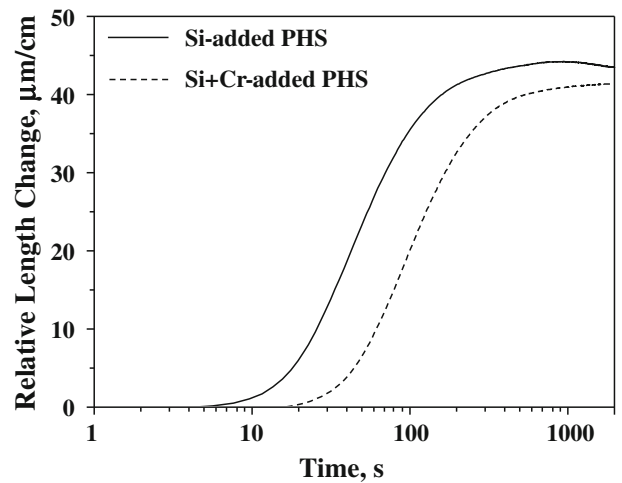


Fig. 14—Dilatometry curves obtained during the isothermal holding of the Si-added and the Si + Cr-added PHS at 673 K (400 °C) for 2000 s after austenitization at 1127 K (900 °C) for 300 s. The observed dilatation is due to the bainite transformation.

1173 K (900 °C) for 300 seconds. The observed change in length is solely due to the formation of bainite, as the selected T_P temperature was between the bainite start temperature, B_s and the M_s temperature. It is clear that less bainite is formed in the case of the Si + Cr-added PHS. Therefore, the volume fraction of decomposed austenite during the partitioning stage is less for the Si + Cr-added PHS.

Cr acts as an austenite stabilizer at low concentrations, and Cr is a well-known ferrite stabilizer at high Cr content.^[14] The small additions of Cr therefore suppressed the decomposition of austenite in the present study.

The original concept of Q&P processing suggested by Speer *et al.*^[19] is based on the two assumptions: (a) the C fully partitions into austenite during the partitioning stage and (b) transformations other than the formation of athermal martensitic do not occur. Consequently, the final microstructure consists of martensite and C-enriched austenite. In the present case, the actual PHS microstructures were different from this ideal case. Figure 15 shows a schematic comparing the microstructure development proposed in the original concept of Q&P processing and the microstructure obtained after Q&P experiments reported in the literature.^[7,15,16,30–32]

Table III lists the microstructures after Q&P processing of various steels as reported in the literature. In the present case and in several earlier studies,^[7,30,31] the occurrence of a bainitic transformation during partitioning stage was reported. In addition, Kim *et al.*^[32] reported an isothermal martensitic transformation occurring during the quenching stage. In the case of highly alloyed steels such as stainless steel,^[15,16] the bainitic transformation did not occur. In the present study, it was shown that the control of the bainitic transformation kinetics during Q&P processing was essential to obtain good mechanical properties. The Q&P model may have to be refined to consider the more complex transformation behavior occurring

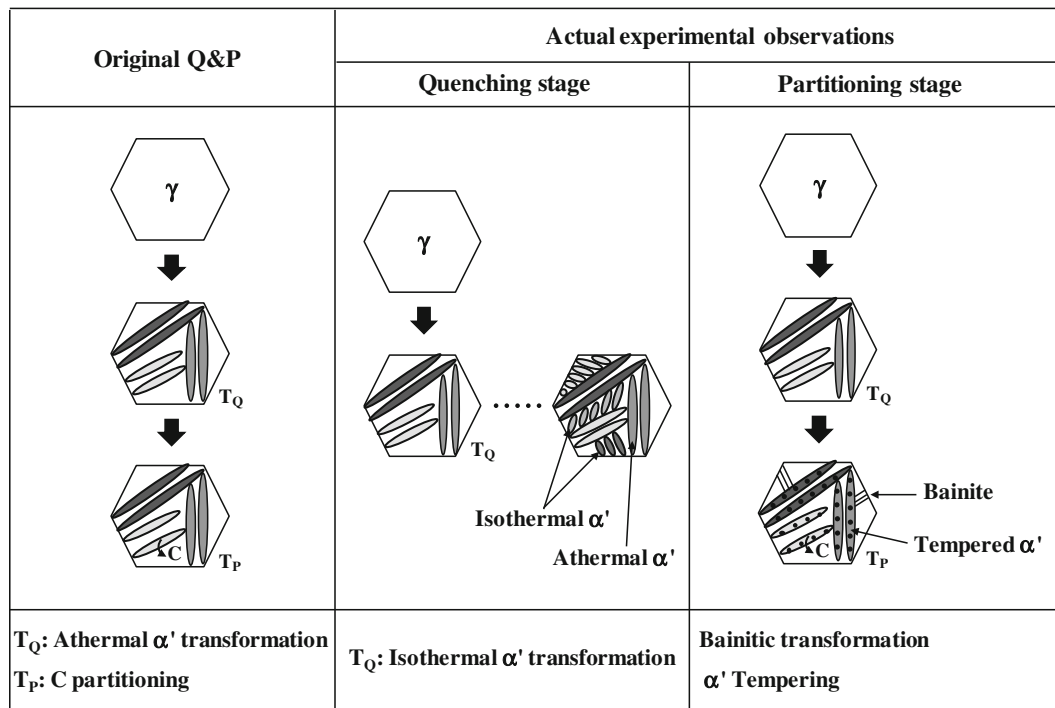


Fig. 15—Comparison between the original Q&P processing concept and the actual experimental observations made during the Q&P processing of Q&P-compatible PHS in the present study. γ and α' represent austenite and martensite, respectively. T_Q and T_P are the Q&P temperatures, respectively.

Table III. Literature Reported Microstructure of Various Q&P-Processed Steels for Different Quenching Temperatures (T_Q) and Partitioning Temperatures (T_P). γ and α' are retained austenite and martensite, respectively

Authors	Steel Composition (Wt Pct)				Microstructure						
	C	Mn	Si	Other	T_Q [K (°C)]	T_P [K (°C)]	Isothermal α'	Bainite	Tempered α'	γ	
Clarke <i>et al.</i> ^[7]	0.19	1.59	1.63	0.036Al	473 (200)	673 (400)	No	Yes	Yes	Yes	
Santofimia <i>et al.</i> ^[30]	0.19	1.61	0.35	1.10Al0.09P	423 (150)	623 (350)	No	Yes	Yes	Yes	
Li <i>et al.</i> ^[31]	0.41	1.3	1.27	0.56Cr1.01Ni	453 (180)	573 (300)	Yes	Yes	Yes	Yes	
Kim <i>et al.</i> ^[32]	0.15	2.06	0.32	0.83Al	623 (350)	623 (350)	Yes	No	Yes	Yes	
Tsuchiyama <i>et al.</i> ^[16]	0.12	0.26	0.87	12.1Cr0.002P	513 (240)	723 (450)	No	No	Yes	Yes	
Mola and De Cooman ^[15]	0.31	0.29	0.47	13.2Cr0.15Ni	338 (65)	723 (450)	No	No	Yes	Yes	
Present study	0.27	1.5	1.61	0.002B	543 (270)	673 (400)	No	Yes	Yes	Yes	
	0.28	1.46	1.58	0.97Cr0.002B	543 (270)	673 (400)	No	Yes	Yes	Yes	

during Q&P processing of steel with a PHS-specific composition.

V. CONCLUSIONS

The Q&P processing concept was applied to alternative Si-added and Si + Cr-added PHS grades. The Q&P-processed PHS had an improved ductility without a loss of strength compared to the conventionally processed 22MnB5 PHS grade. The Q&P processed Si + Cr-added PHS had superior mechanical properties.

The model proposed by Speer *et al.* was slightly modified to take into account the influence of the austenite grain size. The modified model accounts for the absence of secondary martensite (α'_s) during final

quenching, and the increase of the retained austenite volume fraction with increasing quench temperature.

SEM and TEM observations after Q&P processing indicated that the microstructure of the Si-added and the Si + Cr-added PHS had a tempered martensite matrix containing carbide-free bainite and retained austenite islands. The retained austenite was present along the lath boundaries of martensite or as a constituent within the carbide-free bainite. The stability of the retained austenite was very high due to its small grain size and a substantial C-enrichment in the range of 0.9 to 1.7 wt pct. C-enrichment of the austenite was achieved by partitioning and bainite transformation.

The synergetic effect of the Si and Cr additions was significant. Si actively suppressed the carbide formation, resulting in the formation of carbide-free bainite. The addition of Cr resulted in an increase of the retained

austenite volume fraction after Q&P processing. The presence of retained austenite in Q&P processed Si + Cr-added PHS therefore resulted in superior mechanical properties. The Si + Cr-added PHS quenched to 543 K (270 °C) and partition treated at 673 K (400 °C) had a high volume fraction of retained austenite of 0.20. The elongation increased to 17 pct. A combination of a YS of 1098 MPa and an UTS of 1320 MPa was achieved.

ACKNOWLEDGMENTS

The authors gratefully acknowledge the support of Dr. Jin Kuen Oh and Dr. Yeol Rae Cho of the POSCO Technical Research Laboratories, Gwangyang, South Korea.

REFERENCES

1. D.W. Fan, H.S. Kim, and B.C. De Cooman: *Steel Res. Int.*, 2009, vol. 80, pp. 241–48.
2. H. Karbasian and A.E. Tekkaya: *J. Mater. Process. Technol.*, 2010, vol. 210, pp. 2103–18.
3. D.W. Fan, R.B. Park, Y.R. Cho, and B.C. De Cooman: *Steel Res. Int.*, 2010, vol. 81, pp. 292–98.
4. J.G. Speer, E. De Moor, K.O. Findley, D.K. Matlock, B.C. De Cooman, and D.V. Edmonds: *Metall. Mater. Trans. A*, 2011, vol. 42A, pp. 3591–3601.
5. D.V. Edmonds, D.K. Matlock, and J.G. Speer: *La Metallurgia Ital.*, 2011, pp. 41–49.
6. D.V. Edmonds, K. He, F.C. Rizzo, B.C. De Cooman, D.K. Matlock, and J.G. Speer: *Mater. Sci. Eng. A*, 2006, vols. 438–440, pp. 25–34.
7. A.J. Clarke, J.G. Speer, M.K. Miller, R.E. Hackenberg, D.V. Edmonds, D.K. Matlock, F.C. Rizzo, K.D. Clarke, and E. De Moor: *Acta Mater.*, 2008, vol. 56, pp. 16–22.
8. M.J. Santofimia, L. Zhao, R. Petrov, C. Kwakernaak, W.G. Sloof, and J. Sietsma: *Acta Mater.*, 2011, vol. 59, pp. 6059–68.
9. B.C. De Cooman: *Curr. Opin. Solid State Mater. Sci.*, 2004, vol. 8, pp. 285–303.
10. F.G. Caballero, S. Allain, J. Cornide, J.D. Puerta Velásquez, C. Garcia-Mateo, and J.D. Miller: *Mater. Des.*, 2013, vol. 49, pp. 667–80.
11. H.K.D.H. Bhadeshia and D.V. Edmonds: *Metal Sci.*, 1983, vol. 17, pp. 420–25.
12. H.K.D.H. Bhadeshia and D.V. Edmonds: *Metal Sci.*, 1983, vol. 17, pp. 411–19.
13. H.K.D.H. Bhadeshia and D.V. Edmonds: *Metall. Trans. A*, 1979, vol. 10A, pp. 895–907.
14. G. Kirchner, T. Nishizawa, and B. Uhrenius: *Metall. Trans. A*, 1973, vol. 4A, pp. 167–74.
15. J. Mola and B.C. De Cooman: *Metall. Mater. Trans. A*, 2013, vol. 44A, pp. 946–67.
16. T. Tsuchiyama, J. Tobata, T. Tao, N. Nakada, and S. Takaki: *Mater. Sci. Eng. A*, 2012, vol. 532, pp. 585–92.
17. B.D. Cullity and S.R. Stock: *Elements of X-ray Diffraction*, 3rd ed., Prentice-Hall, New Jersey, 2001, pp. 365–69.
18. F. Han, B.C. Hwang, D.W. Suh, Z. Wang, D.L. Lee, and S.J. Kim: *Met. Mater. Int.*, 2008, vol. 14, pp. 667–72.
19. J.G. Speer, F.C. Assunção Rizzo, D.K. Matlock, and D.V. Edmonds: *Mater. Res.*, 2005, vol. 8, pp. 417–23.
20. D.P. Koistinen and R.E. Marburger: *Acta Metall.*, 1959, vol. 7, pp. 59–60.
21. C. Kung and J. Rayment: *Metall. Trans. A*, 1982, vol. 13A, pp. 328–31.
22. A. García-Junceda, C. Capdevila, F.G. Caballero, and C.G. de Andrés: *Scripta Mater.*, 2008, vol. 58, pp. 134–37.
23. E. Jimenez-Melero, N.H. van Dijk, L. Zhao, J. Sietsma, S.E. Offerman, J.P. Wright, and S. van der Zwaag: *Scripta Mater.*, 2007, vol. 56, pp. 421–24.
24. S.J. Lee, S.W. Lee, and B.C. De Cooman: *Int. J. Mater. Res.*, 2013, vol. 104, pp. 423–29.
25. T. Suzuki, Y. Ono, G. Miyamoto, and T. Furuhashi: *ISIJ Int.*, 2010, vol. 50, pp. 1476–82.
26. S.S. Babu, E.D. Specht, S.A. David, E. Karapetrova, P. Zschack, M. Peet, and H.K.D.H. Bhadeshia: *Metall. Mater. Trans. A*, 2005, vol. 36A, pp. 3281–89.
27. E. Kozeschnik and H.K.D.H. Bhadeshia: *Mater. Sci. Technol.*, 2008, vol. 24, pp. 343–47.
28. L. Samek, E. De Moor, J. Penning, and B.C. De Cooman: *Metall. Mater. Trans. A*, 2006, vol. 37A, pp. 109–24.
29. H. Jirková, L. Kučerová, V. Průcha, B. Mašek: *Proc. 21st Int. Conf. Metall. Mater. 2012*, Brno Czech Republic, EU, 2012, TANGER Ltd., pp. 532–38.
30. M. Santofimia, L. Zhao, and J. Sietsma: *Metall. Mater. Trans. A*, 2009, vol. 40A, pp. 46–57.
31. H.Y. Li, X.W. Lu, X.C. Wu, Y.A. Min, and X.J. Jin: *Mater. Sci. Eng. A*, 2010, vol. 527, pp. 6255–59.
32. D.H. Kim, J.G. Speer, H.S. Kim, and B.C. De Cooman: *Metall. Mater. Trans. A*, 2009, vol. 40A, pp. 2048–60.